9

The unified theory of secondary double-diffusive instabilities

In the last three chapters we discussed the major types of large-scale double-diffusive instabilities: collective instability, intrusions and γ-instability. Ironically perhaps, each type has been indentified at some point in history as a precursor of the spontaneous formation of thermohaline staircases. Considerations of clarity forced us to discuss each mode separately, despite the apparent similarities in the formulation of the stability problems and in the analysis. However, a little reflection suggests that at least the linear theory could be united.

The starting point of the unification (Traxler *et al.*, 2011a) is the non-dimensional system (7.1), which has already been used (Chapter 7) to describe interleaving instabilities. This system represents the Boussinesq equations linearized with respect to the motionless basic state uniformly stratified in x and z. The first steps of the unified theory routinely follow the development of all parametric double-diffusive theories (Chapters 6–8). The *T*–*S* fluxes are expressed in terms of the Nusselt number and the flux ratio (6.3), both of which are assumed to be determined by the density ratio. For simplicity, the model is chosen to be two-dimensional although the extension to three dimensions is straightforward. The stability properties of system (7.1) are analyzed using normal modes (7.2), which yields a cubic equation for the growth rate:

$$\lambda^3 + a_2\lambda^2 + a_1\lambda + a_0 = 0. \tag{9.1}$$

The coefficients of (9.1) are given by algebraic expressions in terms of

$$a_i = a_i\left[k, m, \bar{R}_\rho, Nu(\bar{R}_\rho), \gamma(\bar{R}_\rho), G, A_{Nu}, A_\gamma\right]. \tag{9.2}$$

Unlike previous treatments, Traxler *et al.* (2011a) made no attempt to a-priori isolate various types of secondary instabilities. For each value of the background density ratio ($\bar{R}_\rho$), parameters in (9.2) characterizing the patterns of fluxes $\left(Nu, \gamma, A_{Nu}, A_\gamma\right)$ were diagnosed from a series of salt-finger DNS for the oceanographic heat–salt parameters ($Pr = 7, \tau = 0.01$). Then, the growth rate

Downloaded from https://www.cambridge.org/core, on subject to the Cambridge Core terms of use, available at https://www.cambridge.org/core/terms.
https://doi.org/10.1017/CBO9781139034173.010

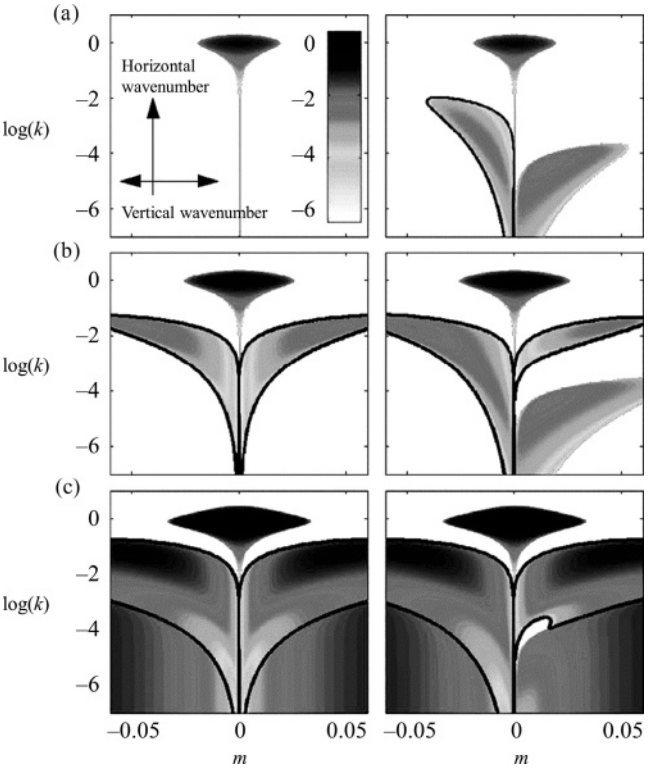

Figure 9.1 The logarithm of the real part of growth rates for the fastest growing perturbations is plotted as a function of wavenumbers. Only positive values of Re(λ) are shown. The horizontal axis shows vertical wavenumber, and the vertical axis shows the logarithm of horizontal wavenumber to capture the broad range of expected scales. The left-hand column shows results in the absence of lateral gradients ($G = 0$), while the right-hand column shows results for $G = 0.01$. Instability regions surrounded by a dark contour show oscillatory behavior. (a) High density ratio ($\bar{R}_\rho = 7$). (b) Mid-range density ratio ($\bar{R}_\rho = 4$). (c) Low density ratio ($\bar{R}_\rho = 1.5$). From Traxler *et al*. (2011a).

equation (9.1) was solved numerically for each wavenumber and the density ratio. The largest real part of its three roots is plotted as a function of the vertical and horizontal wavenumbers in Figure 9.1 for three representative values of $\bar{R}_\rho$. To make the analysis more memorable, Traxler *et al*. (2011a) presented their results in a somewhat peculiar format: the abscissa is the vertical wavenumber and the ordinate is the natural logarithm of horizontal wavenumber. However, the effort was worthwhile – the flower plot in Figure 9.1 is rather amusing.

The interpretation of the unified theory is not as complicated as it might have been since the secondary instabilities generally operate on distinct spatial/temporal scales. As the density ratio decreases, the region of instability systematically grows

Downloaded from https://www.cambridge.org/core, on subject to the Cambridge Core terms of use, available at https://www.cambridge.org/core/terms.
https://doi.org/10.1017/CBO9781139034173.010

and its pattern starts to reveal progressively richer dynamics. To help identify intrusive instabilities, the right (left) panels of Figure 9.1 show the growth rate patterns with (without) the lateral gradients. Figure 9.1a (left) for high density ratio ($\bar{R}_\rho = 7$) contains only one distinct instability region. The "bulb" characterized by the high horizontal wavenumbers is a counterpart of the regular fingering mode. This mode persists, albeit in a quantitatively different form, even when the eddy fluxes are set to zero. Note, however, that the parametric theory cannot accurately represent such small-scale structures since the assumed parameterizations require clear separation between the scales of primary and secondary instabilities. The presence of a lateral gradient introduces (Fig. 9.1a, right panel) two additional regions of instability, one oscillatory and one direct, both confined to large vertical and horizontal scales and appearing as "leaves" in the flower plot. The direct mode corresponds to conventional thermohaline intrusions (Chapter 7). In dimensional units (evaluated for typical oceanic parameters), intrusions in Figure 9.1 typically grow on a time scale of a day, with a horizontal scale of the order of a kilometer and vertical scale of a few meters.

For an intermediate density ratio $\bar{R}_\rho = 4$ (Fig. 9.1b, left) the collective instability waves appear at vertical and horizontal dimensional scales of about a meter, with a growth time scale of about 30 hours. Oscillatory instabilities can be recognized in Figure 9.1 by black contours surrounding the unstable regions. The lateral gradient (Fig. 9.1b, right) strongly modifies the waves, increasing both their maximum growth rate and the size of the instability region for positive slopes, while suppressing growth for negative slopes. The inclusion of the lateral gradient also introduces a direct intrusive mode at much larger horizontal scales.

Finally, at low density ratios, exemplified by the $\bar{R}_\rho = 1.5$ calculation in Figure 9.1c, the system becomes strongly unstable to a continuous range of modes on both horizontal and vertical scales. In this regime, the instabilities are dominated by the collective instability (for intermediate range of horizontal scales) and by the γ-instability for much longer horizontal scales. The largest growth rates are attained by the collective instability, which grows on a time scale of a few hours. The regions occupied by the collective and γ-instabilities are largely unaffected by the presence (absence) of lateral gradients in the right (left) panels of Figure 9.1c. The intrusive zone is completely masked by the encroaching collective instability region. The disappearance of intrusions in the growth rate diagram, however, should not be interpreted as a sign of their insignificance. Even though they grow slowly, mixing driven by intrusions may be substantial (owing to their more effective direct mode of operation) possibly exceeding that of collective instability waves.

Overall, the unified analysis did not fundamentally alter our view of secondary large-scale instabilities but, rather, clarified and sharpened our understanding of

Downloaded from https://www.cambridge.org/core, on subject to the Cambridge Core terms of use, available at https://www.cambridge.org/core/terms.
https://doi.org/10.1017/CBO9781139034173.010

them. Major insights brought by studies of layering, interleaving and collective instabilities in isolation have been confirmed. New twists, such as the sensitivity of the collective instability to lateral T–S gradients and the possibility of the oscillatory intrusive modes, only underscore the richness and complexity of double-diffusive phenomena. It should also be realized that the situation in nature is undoubtedly even more interesting and complicated than in purely double-diffusive models discussed so far. At any given moment, double-diffusive structures in the ocean are forced by ubiquitous large-scale shears, intermittent turbulence and spatial/temporal variability. In the next chapter we attempt to summarize our present, glaringly incomplete, knowledge of the properties of double-diffusion in active environments.

Downloaded from https://www.cambridge.org/core, on subject to the Cambridge Core terms of use, available at https://www.cambridge.org/core/terms.
https://doi.org/10.1017/CBO9781139034173.010